Multicolored Protein Conformation States in the Photocycle of Transducer-Free Sensory Rhodopsin-I

Istvan Szundi, Trevor E. Swartz, and Roberto A. Bogomolni
Department of Chemistry and Biochemistry, University of California, Santa Cruz, Santa Cruz, California 95064 USA

ABSTRACT Sensory rhodopsin-I (SRI), a phototaxis receptor of archaebacteria, is a retinal-binding protein that exists in the cell membrane intimately associated with a signal-transducing protein (HtrI) homologous to eubacterial chemotaxis receptors. Transducer-free sensory rhodopsin-I (fSRI), from cells devoid of HtrI, undergoes a photochemical cycle kinetically different from that of native SRI. We report here on the measurement and analysis of the photochemical kinetics of fSRI reactions in the 350–750-nm spectral range and in a 10^{-7} s to 1 s time window. The lack of specific intermolecular interactions between SRI and HtrI results in early return of the ground form via distinct branching reactions in fSRI, not evident in the photocycle of native SRI. The chromophore transitions are loosely coupled to protein structural transitions. The coexistence of multiple spectral forms within kinetic intermediates is interpreted within the concept of multicolored protein conformational states.

INTRODUCTION

Bacterial rhodopsins function as light energy converters and photoreceptors in *Halobacterium salinarum*. Bacteriorhodopsin (bR) pumps protons and halorhodopsin (hR) transports chloride; sensory rhodopsin-I (SRI) detects both attractant (orange) and repellent (UV-blue) light. Despite their different functions, these proteins have homologous amino acid sequences (Blanck et al., 1989) as well as similar secondary and tertiary structures. All have a retinal chromophore, which is located between transmembrane helixes and is bound to a lysine residue via a Schiff's base linkage. The Schiff's base is protonated in the ground form and has similar protein environments (Fodor et al., 1989), which gives rise to absorption spectra in the 500–600-nm range. The pigments undergo cyclic photoreactions upon illumination and generate electrochemical ion gradients or trigger a signal transduction chain to control the flagellar motor (Hoff et al., 1997; Spudich, 1993; Schobert and Lanyi, 1982; Oesterhelt and Stoeckenius, 1973; Lozier et al., 1975). Photoexcitation is followed by a series of dark reactions producing a number of intermediate states, which are named K, L, M, N, and O in the best known bR photocycle.

In its native environment, SRI is associated with a membrane-bound signal transducer protein, HtrI, which is homologous to eubacterial chemotaxis receptors (Yao and Spudich, 1992). The intermediate states in the photocycle of SRI, $S_{610}/S_{560}/S_{373}$, (Bogomolni and Spudich, 1987) are analogous to K, L, and M states of the bR photocycle, and their kinetics are independent of pH (Olson and Spudich, 1993). No external release or uptake of protons is detected during the lifetime of SRI^{M}_{373}, and it is believed that proton transfer reactions that inevitably accompany the deprotonation and protonation of the Schiff's base occur entirely within the membrane (Bogomolni and Spudich, 1982; Spudich and Spudich, 1982).

When SRI is expressed in cells devoid of HtrI and a transducer-free sensory rhodopsin, fSRI, is produced, the photochemistry of the pigment seems to change significantly. The decay of the $fSRI^{M}$ state becomes highly pH dependent, and protons are released transiently during the lifetime of $fSRI^{M}$ (Spudich and Spudich, 1993; Olson and Spudich, 1993; Jung et al., 1999). We have shown (Bogomolni et al., 1994) that fSRI exists in two forms in a pH-dependent equilibrium with pK = 7.2. The base form, $fSRI_{550}$, functions as a light-driven electrogenic proton pump, similarly to bR, whereas the acid form, $fSRI_{587}$, shows only transient proton release and uptake. We suggested that protonation of Asp76 residue in $fSRI_{587}$, as in native SRI (Bousché et al., 1991; Rath et al., 1994), prevents proton pumping by this form and brings about absorption characteristics similar to SRI.

Here we report on the photocycle of $fSRI_{587}$ and show that despite the spectral resemblance of this form to native SRI, there are significant differences in their photo conversions. Our results indicate that interactions between the light sensor and the transducer are already manifested in the early steps of photochemistry.

MATERIALS AND METHODS

Vesicles containing fSRI were prepared as described elsewhere (Bogomolni et al., 1994). The pH of the vesicle suspension in 4 M NaCl was adjusted to 5.3 by adding small amounts of HCl or NaOH. Repetitive measurements on the same sample volume cannot be carried out conveniently because of the long decay times of intermediates in the photocycle. To overcome this problem, a pulse flow system was designed, in which the photolyzed sample in the measuring cell was replaced with a fresh one after each laser excitation. The pulse flow system utilizes a commercial peristaltic pump with logic control (Pharmacia model P-1, Uppsala, Sweden) connected to a homemade flow cell of 5-mm optical path length and 15-μl

Received for publication 12 June 2000 and in final form 12 October 2000.
Address reprint requests to Dr. Roberto A. Bogomolni, Department of Chemistry and Biochemistry, University of California, Santa Cruz, 1156 High Street, Santa Cruz, CA 95064. Tel.: 831-459-4294; Fax: 831-459-2935; E-mail: bogo@chemistry.ucsc.edu.

0006-3495/01/01/469/11 $2.00

sample volume. The cell design is similar to the one described by Lewis and Kliger (1993). To ensure complete displacement of the photolyzed sample, 30 μl of fresh sample were pumped through the measuring cell in each flow pulse. All absorbance measurements were carried out at room temperature (22°C).

Light-induced absorbance changes were measured in the 350–750-nm spectral range with a gated optical multichannel analyzer (OMA) (EG&G PAR, Princeton, NJ) attached to a Jarrell-Ash monochromator (MonoSpec 27, Waltham, MA). Gate pulses of 10 ns duration were delivered by a high-voltage fast pulser (EG&G PAR model 1302). The 10-ns green light pulse of a Nd:Yag laser equipped with frequency doubler (Quanta-Ray model DCR-1A, Mountain View, CA) was used to excite the sample, and a microsecond Xe-flash lamp (EG&G model FX-800) powered by a high-voltage laboratory power supply (EG&G PAR model PS-302) provided the white measuring pulse. The time delays of probing, following the laser excitation pulse, were arranged in a quasi-logarithmic fashion at values of 1, 2, and 5 in each decade on the time scale from 100 ns to 1 s. Filters placed in the path of the probe beam were used to optimize the spectral distribution of the measuring light.

Actinic and probe beams entered the sample in a 90° geometry. To avoid complications due to the linearly polarized actinic beam, all measurements were done at saturating laser intensities. Control experimental data taken at parallel and perpendicular polarization of the measuring beam relative to the actinic polarization axis showed no noticeable differences. A pulse-delay generator (Stanford Research System model DG535, Sunnyvale, CA) was used to synchronize the OMA, gate pulse generator, laser, and probe lamp.

The OMA data acquisition program included the following steps in each data collection sequence: taking dark background readings, measuring probe beam intensities before and after laser excitation, and providing appropriate logic pulses through the PIA port of the OMA for the operation of the peristaltic pump and the shutters that controlled the passage of laser and probe beam pulses to the sample. The experimental difference spectra reported here are averages of 100 data collection sequences taken in groups of 5 or 10. In each group, the light intensities were averaged to calculate an absorption difference spectrum. Difference spectra falling into a preset accuracy range were accumulated until the desired number of scans was completed. This procedure provided a useful filter to reject inaccurate readings should any malfunction of the measuring system occur. The absorbance data were transferred to a PC computer for further analysis by programs written in Matlab environment (The Math Works, Natick, MA).

Data analysis

Global exponential fit

Assuming that the dark reactions following the laser excitation are first-order chemical reactions, the absorption difference spectra, $\Delta a(\lambda,t)$ are represented by a sum of exponentials of the following form:

$$\Delta \boldsymbol{a}(\lambda, t) = \sum_i \boldsymbol{b}_i(\lambda)\exp(-r_i t) + \boldsymbol{b}_0(\lambda), \qquad (1)$$

where r_i represents the experimental decay constants or apparent rate constants, and the amplitudes of the time-dependent, $\boldsymbol{b}_i(\lambda)$, and time-independent, $\boldsymbol{b}_0(\lambda)$, components are referred to as b-spectra.

To perform the global exponential fit the absorption difference spectra taken at different time delays following the laser excitation pulse are arranged in the columns of a data matrix, $\Delta\boldsymbol{a}(\lambda,t)$. The data matrix is subject to singular value decomposition (SVD): $\Delta\boldsymbol{a}(\lambda,t) = \boldsymbol{USV}'$. Nonsignificant vectors displaying only noise are excluded from further analysis by cutting the component matrices produced by SVD according to the number of basis vectors kept.

The time-dependent component matrix, $\boldsymbol{V}$, from SVD is fit to a sum of exponentials using a Nelder-Meade simplex algorithm, and the apparent rates are obtained. The spectra associated with each exponential term at the given set of wavelengths are calculated using the $\boldsymbol{U}$ and $\boldsymbol{S}$ component matrices as described by Hug et al. (1990).

The apparent rates and b-spectra of the global exponential fit are related to the microscopic reaction rates using the algebraic methods described previously (Thorgeirsson et al., 1993; Nagle, 1991; Szundi et al., 1997). A brief summary of the method is given below. A reaction scheme involving n intermediates is described by a set of first-order differential equations:

$$\boldsymbol{c}(t)' = \boldsymbol{K}\boldsymbol{c}(t)', \qquad (2)$$

where $\boldsymbol{c}(t)$ is the concentration column vector of length n, $\boldsymbol{c}(t)'$ is its time derivative, and $\boldsymbol{K}$ is the kinetic matrix composed of the microscopic rate constants. The general solution to the set of differential equations is a sum of exponentials:

$$\boldsymbol{c}(t) = \sum_i \boldsymbol{p}_i \exp(\alpha_i t), \qquad (3)$$

where α_i are the eigenvalues of the kinetic matrix. The preexponential factors, $\boldsymbol{p}_i$, are related to the eigenvectors, $\boldsymbol{v}_i$, through a scalar scaling factor, f_i, obtained from the concentration vector at zero time:

$$\boldsymbol{p}_i = f_i \boldsymbol{v}_i. \qquad (4)$$

Because of the mass conservation law, the kinetic matrix is singular, and one of its eigenvalues is zero. The corresponding eigenvector, $\boldsymbol{v}_0$, describes a time-independent state. The time-dependent absorption difference spectra, $\Delta\boldsymbol{a}(\lambda,t)$, in practice can be written as

$$\Delta \boldsymbol{a}(\lambda, t) = \varepsilon(\lambda)\left(\sum_i f_i \boldsymbol{v}_i \exp(\alpha_i t) - \boldsymbol{c}_{bl}\right), \qquad (5)$$

where $\boldsymbol{c}_{bl}$ is the concentration vector of the photolysed (bleached) components and $\epsilon(\lambda)$ is a matrix describing the extinction coefficients of the intermediates. It follows from Eqs. 1 and 5 that the apparent rate constants are the eigenvalues taken with negative signs, and the experimental b-spectra are linear combinations of the intermediate spectra:

$$\boldsymbol{b}_i = \varepsilon(\lambda) f_i \boldsymbol{v}_i \qquad (6)$$

$$\boldsymbol{b}_0 = \varepsilon(\lambda)(f_0 \boldsymbol{v}_0 - \boldsymbol{c}_{bl}). \qquad (7)$$

The b_0-spectrum represents the difference between the spectra of the final photoproduct, $f_0\ \boldsymbol{v}_0$, and the photolysed pigment, $\boldsymbol{c}_{bl}$, and it is zero for a cyclic process. The b-spectra contain the information about the eigenvectors of the kinetic matrix.

Reconstruction of kinetic schemes from b-spectra

The kinetic matrix can be reconstructed from its distinct eigenvalues and the corresponding independent eigenvectors. We use the results of the global exponential fit to construct kinetic schemes, which are consistent with our expectations about the spectra of the intermediates. The apparent rates from the global exponential fit provide a set of experimental eigenvalues, which are used as the distinct eigenvalues of the unknown kinetic matrix. The experimental b-spectra are decomposed into individual spectral components, believed to represent the spectra of intermediates, and the amplitudes of the components are arranged in a composition matrix. The composition matrix is expected to represent the eigenvector matrix of the unknown kinetic matrix. Its columns and rows should satisfy the balance requirements derived for the eigenvector matrix of a kinetic matrix. The balance equations relate the amplitudes within each b-spectrum (Eq. 8) and the amplitudes of each intermediate in the different b-spectra (Eq. 9)

(Szundi et al., 1997):

$$\sum_{j} \boldsymbol{v}_{ji} = 0 \tag{8}$$

$$\sum_{i} f_i \boldsymbol{v}_{ji} = \boldsymbol{c}_j(t = 0). \tag{9}$$

Eq. 9 shows that the concentration vector has zero values for each intermediate that is not present at zero time; therefore, these intermediates should be present in more than one of the b-spectra. An approximately balanced composition matrix is considered a trial or experimental eigenvector matrix. A kinetic matrix is calculated from the experimental eigenvalues and eigenvectors:

$$\boldsymbol{K} = \boldsymbol{V}\,\alpha\,\boldsymbol{V}^{-1}, \tag{10}$$

where α is a diagonal matrix containing the experimental eigenvalues, and $\boldsymbol{V}$ is the experimental eigenvector matrix. The final eigenvector matrix is usually the result of a number of refinements, necessary to produce the simplest numerically balanced kinetic matrix with physically meaningful microscopic rates. Not every experimental eigenvector matrix with formally balanced columns and rows produces a physically meaningful kinetic matrix. In that case the experimental eigenvector matrix is not a proper eigenvector matrix for a kinetic scheme, and the kinetic components in the b-spectra should be redefined.

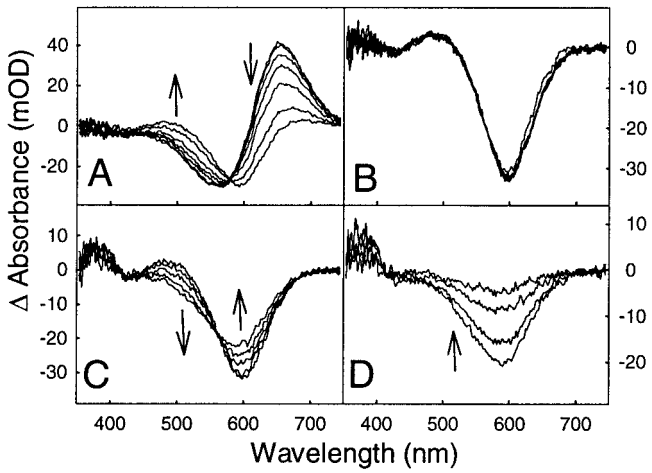

FIGURE 1 Difference absorbance spectra for transducer-free sensory rhodoposin-I (fSRI) measured at pH 5.3 and at time delays from 100 ns to 1 s following 532-nm laser excitation. Arrows indicate the direction of absorbance changes in time. (*A*) Times of 100, 200, and 500 ns and 1, 2, 5, and 10 μs. (*B*) Times of 20, 50, 100, 200, and 500 μs and 1 ms. (*C*) Times of 2, 5, 10, 20, and 50 ms. (*D*) Times of 100, 200, and 500 ms and 1 s.

RESULTS AND DISCUSSION

Global exponential fit

The number of data points collected at 678 wavelength values was reduced to 226 by point averaging. The absorption curves were corrected for the slight baseline drifts, which cannot be ignored at low signal levels. Absorption spectra taken at 22 time delays were arranged in a 226 × 22 data matrix. The experimental data, arranged in four panels for clarity, are shown in Fig. 1. In the first 10-μs time window, a red-absorbing form decays to a blue-absorbing one. Little change occurs in the next time window, from 10 μs to 2 ms. In the 2–50-ms time range, a 380-nm form appears and then decays to the ground form in fractions of a second.

Singular value decomposition of the data matrix showed three or possibly four components above noise level. Because SVD, when applied to noisy experimental data, tends to underestimate the number of intermediates the number of basis vectors was set to six. Global exponential fitting using two decay constants does not eliminate all spectral features from the residuals. Fitting with three exponentials reduces the average residuals per point significantly (Table 1), but the residuals still show some spectral features present in the microsecond region (Fig. 2 *B*). Fitting with four exponentials gives slightly lower value for the average residuals per point and removes spectral features from the residuals. The first two decay constants are in the time range of the first transition seen for the three-exponential fit, separating the first transition into two steps. Both the amplitude and the spectral shape of the first and second b-spectra are very similar (Fig. 2 *C*). The noise below 400 nm is higher than in the other spectral regions due to low light intensity; therefore, the shapes of the intermediate spectra are less certain at the low wavelength edge, particularly for small-amplitude components.

If the number of intermediates is small, and they are well separated in time, the b-spectra can be interpreted in a straightforward way (Szundi et al., 1997). The general, though quite simplified, rule is the following: intermediates that decay in a transition contribute to the b-spectrum with positive amplitudes, and intermediates that grow contribute with negative amplitudes. The first b-spectrum of the three-exponential fit describes the conversion of a red-absorbing form into a blue-absorbing one, which is analogous to the K-to-L transition in the bR photocycle. In the second b-spectrum, the blue-absorbing form then decays to two forms: one absorbing around 600 nm and one around 380 nm. The latter form is an unprotonated Schiff's base, analogous to the M intermediate of bR. In the last transition, this 380-nm form decays into the ground form. The four-exponential fit is interpreted in a similar way.

Spectral forms from b-spectra indicate shortcuts from intermediates to the ground form

Because the first two b-spectra of the four exponential fit appear to involve the same intermediate spectra, for the discussion of the possible intermediate forms, we begin by

TABLE 1 Global exponential fit

Tau				Residual per point
	4.1 μs		260 ms	$2.6\ 10^{-4}$
	4.4 μs	17 ms	520 ms	$5.0\ 10^{-5}$
2.2 μs	9.5 μs	16 ms	530 ms	$3.0\ 10^{-5}$

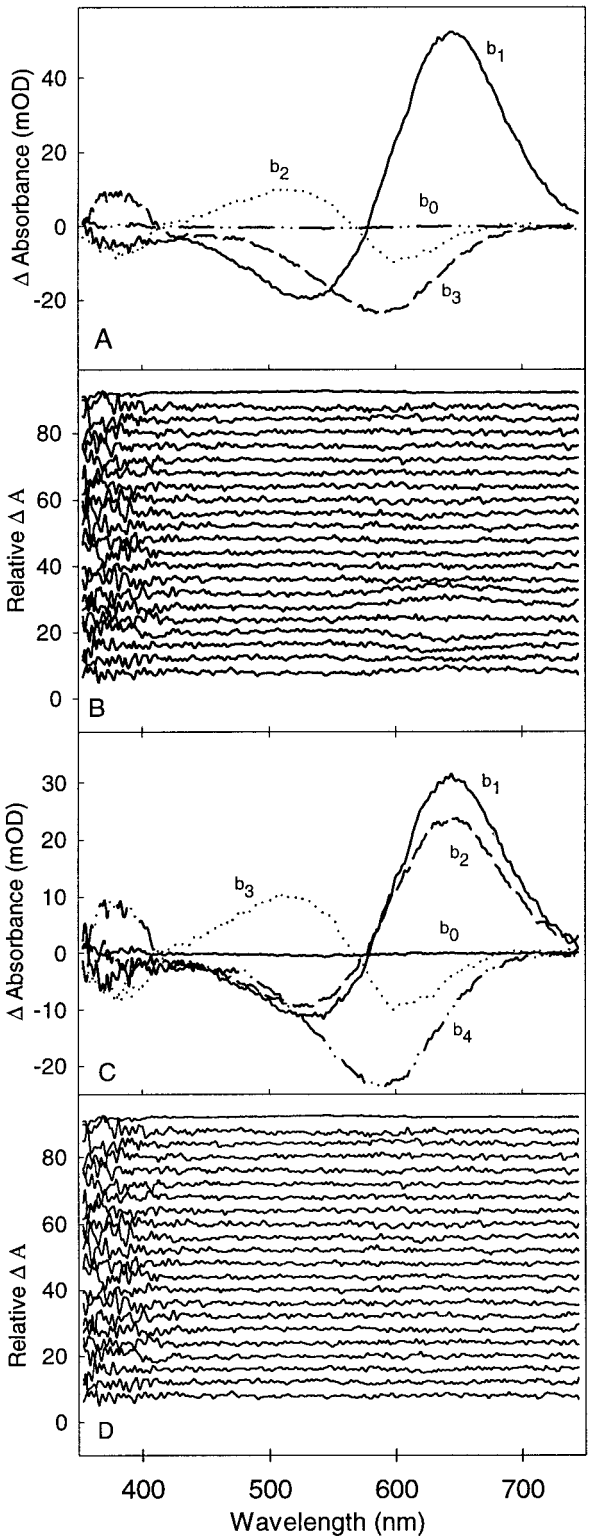

FIGURE 2 Spectral changes (*A* and *C*) and residuals (*B* and *D*) obtained by global exponential fitting following SVD analysis of the data matrix. The b-spectra of the three-exponential fit with 4.4-μs, 17-ms, and 520-ms apparent lifetimes (*A*) and the corresponding residuals (*B*). The b-spectra for the four-exponential fit with 2.2-μs, 9.5-μs, 16-ms, and 530-ms apparent lifetimes (*C*) and the corresponding residuals (*D*). b_0 is the time-independent b-spectrum. Residuals are displaced by 5 mOD for clarity.

using the b-spectra of the three-exponential fit. The interpretation of the last b-spectrum is the most straightforward, because it describes the recovery of the ground form from the M-like intermediate. The spectral shape of the ground form can be reproduced by a skewed Gaussian with maximum at 587 nm. This shape is remarkably similar to the absorption spectrum of bR and to that of bovine rhodopsin (except for its λ_{max}). It can be reproduced by adding minor components to a main Gaussian spectrum and combining the latter with a broad spectrum centered at 360 nm to account for the so-called *cis*-band; 23 mOD of this spectral form fills in the trough of the last b-spectrum (Fig. 3 *A*). The remaining spectral shape is that of the M-like form with unprotonated Schiff's base, which can also be obtained with higher spectral resolution from prolonged illumination of the sample. The spectrum of this M-like form was recorded in a diode array spectrophotometer and appeared to have vibronic structure, similar to what is found for the M-form of SRI at low temperatures (Ariki et al., 1987). It can be reproduced by combining three Gaussian shapes with the central one located at 373 nm. The reproduced spectral shape shown also in the figure will be used in the analysis of the kinetic scheme.

The 23-mOD amplitude of the ground form recovered in the last step is not enough to compensate for the amount of bleached ground form missing in the first experimental absorption difference spectrum recorded at 100 ns following the laser excitation. A minimum of 43 mOD of the ground form is required to eliminate the negative absorbance in that

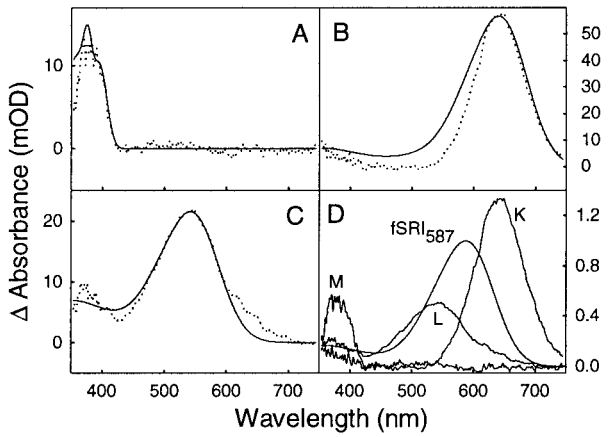

FIGURE 3 Evidence for shortcuts to the ground form. Comparison of intermediate spectral forms (···) produced by adding $fSRI_{587}$ absorption to eliminate negative absorbance, and the corresponding model spectral shapes (——). (*A*) M-like form obtained from the third b-spectrum of the three-exponential fit by adding 23 mOD of $fSRI_{587}$. (*B*) K-like intermediate obtained by adding 43 mOD of $fSRI_{587}$ to the difference spectrum measured at 100-ns delay. (*C*) L-like form obtained by adding 43 mOD $fSRI_{587}$ to the sum of the second and third b-spectra of the three-exponential fit. Normalized spectra of the intermediate forms and the $fSRI_{587}$ ground form (*D*) show the spectral width and amplitude anomalies of the intermediate spectra without considering shortcuts to the $fSRI_{587}$ ground form.

difference spectrum; therefore, 20 mOD of the ground form must be recovered in the earlier steps. The spectrum of the first recorded intermediate, a K-like form, obtained after adding 43 mOD of the ground form to the first experimental spectrum, is shown in Fig. 3 *B*. Its maximum is at 640 nm and its shape appears to narrow as is apparent when it is compared with the spectrum of the ground form with a 640-nm maximum, which is also depicted.

The shape of the b_2-spectrum suggests that part of the ground form is recovered in this step. Indeed, the trough seen at 600 nm in this b-spectrum must be the ground form, as no other 600-nm form appears as a positive component in any of the b-spectra. Based on the balance equation of the eigenvector matrix discussed above, each negative component associated with an intermediate present in a b-spectrum must be compensated for with a positive component present in another b-spectrum. The simplest way to determine the spectral shape of the blue-absorbing L-like form is to combine the b_2- and b_3-spectra and then add 43 mOD of the ground form. By combining the last two b-spectra, we practically eliminate the formation and decay of the M-like form, thus connecting the L-like form directly to the ground form. The spectrum of the L-like intermediate is centered at 542 nm and is shown in Fig. 3 *C*. Again, for comparison, the shape of the ground form spectrum is also shown. The spectra of the K-, L-, and M-like intermediates, normalized by the corresponding mOD values of the ground form, are shown together with the ground form in Fig. 3 *D*.

Traditional models do not produce acceptable intermediate spectra

The step-by-step derivation of these spectral shapes is equivalent to proposing a sequential K→L→M→SRI mechanism with an additional L→SRI branch. The acceptance or rejection of this scheme can be based only on the quality of the intermediate spectra, because we have no clue to judge the validity of the microscopic rates in the model.

The L-like intermediate spectrum has an acceptable spectral width and an additional red tail, which can probably be removed by introducing a reversible step between the K- and L-like intermediates. The main reason why these schemes cannot be accepted is the narrow spectrum of the K-like intermediate. This spectral shape is distinctly different not only from the spectral shapes of the ground forms of the rhodopsin family but also from the spectral shapes of all accepted intermediates. The spectra of the intermediates and the ground forms of the rhodopsin family possess a characteristic common feature. When displayed on the wavenumber (energy) rather than the wavelength scale, the widths of the intermediate and ground form spectra are remarkably similar, and all the spectra can be derived essentially from a single standard form. Although the absorption maximum (energy gap), is very sensitive to the presence of a single charged group on or around the retinal chromophore (opsin shift), the width (energy distribution) is determined by the rotational and vibrational transitions of all the atoms in the chromophore, as well as by interactions with all the neighboring atoms of the surrounding medium, which leads to the well known spectral broadening. It is therefore expected that the widths of the intermediate spectra would not differ significantly from the width of the ground form spectrum, and narrowing of the spectral shape is particularly unlikely. Intermediate spectra are usually somewhat broader than the ground form spectrum, indicating that the inhomogeneity of the medium around the chromophore may become slightly higher during the relatively short lifetimes of the intermediates. The spectrum of the K-like intermediate is unacceptable because its width is only 70% of the width of the ground form. Because the K-like intermediate is the first one in the measurement time window, its spectrum is solely determined by the first recorded experimental difference spectrum and the amplitude of the ground form spectrum added to it. The arrangement of the reaction steps in the kinetic scheme has no effect on this spectrum.

The width of the K-like intermediate becomes acceptable only when substantially higher amounts of the ground form spectrum are added to the first recorded difference spectrum. This is equivalent to a shortcut from this intermediate to the ground form in the scheme because the L→SRI branch cannot take more ground form without sacrificing the width of the L spectrum. The final scheme then becomes a sequential K↔L→M→SRI mechanism with additional K→SRI and L→SRI branches to account for the shortcuts and the back reaction mentioned above. The early shortcut is complete within a couple of microseconds and the L-like intermediate decays in tens of milliseconds according to the results of the three-exponential fit, which is clearly inconsistent with the reversibility of the K-to-L transition. Therefore, the scheme with the back reaction is rejected. Without the back reaction, however, the L-like intermediate has a red tail and cannot be accepted. Below we demonstrate in a general way that the results of the global exponential fit are inconsistent with the presence of the four intermediates having acceptable standard spectral shapes.

Decomposition of the experimental b-spectra into spectral components

Spectral shape of the presumed intermediates

The spectrum of the ground form and the distinct spectral shape of the M-like intermediate were already described above. Our expectation is that the spectral shapes of the other intermediates mimic the shape of the absorption spectrum of the ground form, a general tendency observed in the photochemistry of rhodopsin and bacteriorhodopsin. We calculate the intermediate spectra as sums of Gaussians with two major components as already described for the ground

form. Additional minor components with parameters fixed to those of the two major Gaussian components ensure a fine reproduction of the skewed Gaussian shape of the main absorption band and the relatively constant value of absorbance in the *cis* band. The position, width, and relative amplitude of the main band are adjusted to produce the desired spectra of the intermediates.

Composition of b-spectra of the three- and four-exponential fits

The first b-spectrum in the three-exponential fit can be decomposed into three major components with absorption maxima at 620, 587, and 540 nm (Fig. 4). The amplitude of the fourth M-like component is small. The 620-nm component has positive amplitude; all the other components have negative ones. The simple interpretation of this b-spectrum is the simultaneous transition of a K-like form into both an L-like one and into the ground form. A small amount of an M-like form is also produced. The decomposition of the first b-spectrum thus confirms that introduction of a shortcut to the ground form from the first intermediate restores the shape of the K-form and lowers its amplitude. The width of the L-like model spectrum on the wavelength scale is the same as that of the ground form, 55 nm, whereas the K-like model spectrum is slightly broader, 60 nm, as expected for a spectrum with absorption maximum at a longer wavelength. In analogy with bacteriorhodopsin nomenclature, these intermediate forms will be called $fSRI^{K}_{620}$, $fSRI^{L}_{540}$, $fSRI^{M}_{373}$, and $fSRI_{587}$. The second b-spectrum corresponding to the 16.8-ms decay time contains the same four spectral forms already mentioned. The fit at 600 nm and above was not satisfactory if the $fSRI^{K}_{620}$ form was omitted. The $fSRI^{L}_{540}$ is the main decaying component, which was formed in the previous transitions; the small amount of $fSRI^{K}_{620}$ is a leftover from the earlier conversion of this form. This transition produces roughly equal amounts of $fSRI^{M}_{373}$ and the ground form.

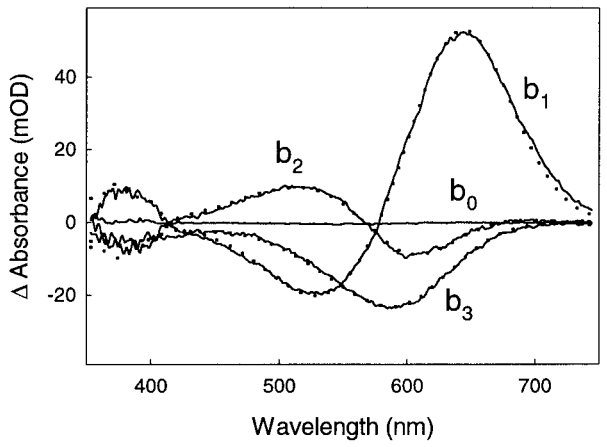

FIGURE 4 Decomposition of b-spectra of the three-exponential fit into single-color-component spectra with λ_{max} at 620, 587, 540, and 373 nm. The spectral shapes of the 620-, 587-, and 540-nm components resemble the shapes of the ground form and are skewed Gaussians with 60-, 55-, and 55-nm bandwidths and 0.9, 1.0, and 0.6 relative amplitudes, respectively. The 373-nm component is a reproduced shape of the experimental M-like form. The composition matrix shows a reasonable amplitude balance and the reproduced (···) and the experimental (——) b-spectra agree reasonably well.

The last b-spectrum contains $fSRI^{M}_{373}$ with positive amplitude and the ground form with negative amplitude and can be interpreted as the recovery of the last portion of the bleached ground form. A reasonable balance of components is achieved throughout the b-spectra decomposition if the amplitudes of the $fSRI^{K}_{620}$, $fSRI^{L}_{540}$, and $fSRI^{M}_{373}$ intermediates relative to the ground form are 0.9, 0.6, and 0.7, respectively.

The composition of b-spectra of the four-exponential fit was obtained in a similar way, and as expected, the first and second b-spectra differ only slightly. The four model spectra were sufficient to decompose all four b-spectra.

Derivation of the kinetic matrix from the components of the b-spectra

Each b-spectrum is a piece of the kinetic scheme, and the whole scheme can be put together from these pieces by trial and error. The microscopic rate constants in the scheme can be adjusted to provide an adequate fit to the b-spectra and the apparent rates. Finally, calculation of the intermediate spectra from the kinetic matrix and the b-spectra can be used to test the validity of the constructed scheme. There is, however, a way to obtain the kinetic matrix from the experimental eigenvalues and the eigenvectors directly (Szundi et al., 1997). The results of b-spectra decomposition are summarized in Table 2. If we intend to use the results of decomposition for the four-exponential fit to calculate the kinetic matrix, we have to face the following problem: three intermediates and a ground form can produce only three exponential decay constants and their corresponding b-spectra. Four apparent rates and b-spectra can be explained only by the presence of an isospectral intermediate, which is difficult to handle even for three apparent rates (Szundi et al., 1997). Therefore, we proceed by doing the calculation for the three-exponential fit, which is consistent with the number of intermediates and only slightly inferior

TABLE 2 Composition of b-spectra

	Three-exponential fit			Four-exponential fit			
	b_1	b_2	b_3	b_1	b_2	b_3	b_4
$fSRI^{K}_{620}$	97	5.3	0	58	41	4.8	0
$fSRI^{L}_{540}$	−31	32	0	−17	−16	34	0
$fSRI^{M}_{373}$	−7.6	−15	21.1	−5.0	−1.0	−17	23
$fSRI_{587}$	−56	−21	−23.1	−34	−23	−22	−23

Amplitudes are in mOD.

to the four-exponential fit. The amount of the recovered ground form was calculated as the sum of the last entries in columns one to three and was included in a fourth column with opposite sign. The four columns of amplitudes make a 4 by 4 matrix $\boldsymbol{V}$, which is our trial or experimental eigenvector matrix to be used in the calculation of the kinetic scheme according to Eq. 10. The first three elements of the diagonal matrix α in that equation are the inverse of the decay time constants of the three-exponential fit taken with negative sign; the fourth element is zero. The elements of the calculated kinetic matrix, the microscopic rate constants, are in Table 3.

The nondiagonal elements of the kinetic matrix are the microscopic rate constants of the reactions in the corresponding kinetic scheme. Each column in the kinetic matrix contains microscopic rates of conversion of an intermediate into all the others. For example, the numbers in the first column show the rate of conversion of the first intermediate of the scheme into second, third, etc. intermediates. Similarly, the second column contains the rate of conversion of the second intermediate to the first (back-reaction) and third, fourth, etc. intermediates.

The second column has physically meaningless large negative rate constants corresponding to the decay of $fSRI^{L}_{540}$ to $fSRI_{373}$ and the ground form. These big negative rates are compensated by a large positive rate for a back reaction from $fSRI^{L}_{540}$ to $fSRI^{K}_{620}$. The physically meaningless negative rates together with the large positive rates indicate that the kinetics cannot be described by the four intermediates. Note that this conclusion is not limited to a particular kinetic scheme; on the contrary, it states that there is no scheme that can produce the composition of the b-spectra described above. The reason behind this statement is simple. In the formal interpretation of schemes, the presence of a small amount of the first $fSRI^{K}_{620}$ intermediate at late times, together with the second intermediate $fSRI^{L}_{540}$, requires a forward-shifted equilibrium between $fSRI^{K}_{620}$ and $fSRI^{L}_{540}$ in the first step. Because of the fast shortcut to the ground form from the $fSRI^{K}_{620}$ intermediate in the first step, however, such an equilibrium cannot physically maintain any significant amount of $fSRI^{K}_{620}$ at late times. This inconsistency also holds for the four-exponential fit and cannot be resolved within the framework of the four intermediates discussed above. To solve the problem of rates, we are forced to assume kinetically different but spectrally similar intermediates for both the $fSRI^{K}_{620}$ and the $fSRI^{L}_{540}$ forms. In the past, the technique of b-spectra decomposition and kinetic matrix calculation worked well for the analysis of rhodopsin kinetics, and we were able to describe one pair of isospectral intermediates quantitatively (Szundi et al., 1997). An extension of that approach to a region of analysis of two pairs of coexisting isospectral intermediates, however, is very difficult. In our attempt to describe the kinetics of $fSRI_{587}$, we have used traditional kinetic analysis ideas that assume that each color form derived from the experimental data corresponds to a distinct kinetic intermediate. We propose that this principle does not hold true in the photoreactions of $fSRI_{587}$, creating enormous complexity in the kinetics when traditional analysis is applied. We suggest an alternative approach to describe the kinetics of this protein using the ideas of multicolor conformational states.

TABLE 3 Microscopic rate constants (s^{-1}) of the calculated kinetic matrix: three-exponential fit

	$fSRI^{K}_{620}$	$fSRI^{L}_{540}$	$fSRI^{M}_{373}$	$fSRI_{587}$
$fSRI^{K}_{620}$	$-2.2\ 10^5$	$3.6\ 10^4$	0	0
$fSRI^{L}_{540}$	$7.1\ 10^4$	$-1.2\ 10^4$	0	0
$fSRI^{M}_{373}$	$1.7\ 10^4$	$-2.8\ 10^3$	−1.9	0
$fSRI_{587}$	$1.3\ 10^5$	$-2.1\ 10^4$	2.1	0

The concept of multicolor conformational states

The continued presence of the $fSRI^{K}_{630}$ and $fSRI^{L}_{540}$ forms in different ratios in a broad time range suggests that factors that determine the chromophore color may not always determine the state of the kinetic intermediate. In other words, the difference in color does not necessarily mean a significant change in the total energy of the protein, and protein states with different energies may have the same color. Examples of the latter case are the early and late deprotonated Schiff's base intermediates in rhodopsin kinetics (Thorgeirsson et al., 1992) and the optically silent transitions detected by nonoptical techniques. The energy surface that controls the movement of the system along the reaction path is a collection of valleys separated by hills of different altitudes. Depending on how deep these energy valleys are and how they are connected, the system may follow a well-defined unidirectional path or may go in more than one direction at a time.

When $fSRI^{K}_{620}$ and $fSRI^{L}_{540}$ color states coexist in time, it indicates that these states have similar energy levels and are separated by low-energy barriers. Despite the significant difference in color, these states can be envisaged as two relatively shallow riverbeds that run parallel on the bottom of a deeper valley connecting the kinetic intermediates, the conformational states on the energy surface. We describe the kinetics of conversions between conformational states rather than individual color states. We combine the energetically similar K and L states into one mixed multicolor state, a protein conformational state $P\text{-}I^{KL}$, which has a broader spectrum than the usual single-color states. Obviously, these conformational states must have some differences in color, because our measurement technique detects only color changes. We can identify four and five conformational states for the three- and four-exponential fits, respectively.

For the three-exponential fit, $P\text{-}I^{K}_{1}$ is the same as $fSRI^{K}_{620}$, $P\text{-}I^{KL}_{2}$ is a mixture of $fSRI^{K}_{620}$ and $fSRI^{L}_{540}$, $P\text{-}I^{M}_{3}$ is $fSRI^{M}_{373}$, and $P\text{-}I^{fSRI}_{4}$ is the ground form $fSRI_{587}$. The matrix of scaled

eigenvectors for the new reaction components is shown in Table 4. Because intermediates P-I_3^M and P-I_4^{fSRI} did not change, their amounts are the same as already given in the composition of b-spectra. It is the amount of the first and second intermediates that needed to be recalculated because of the multicolored new states. The first element of column 1 (Table 6), the amplitude of P-I_1^K, is the total amount of $fSRI_{620}^K$ present in all b-spectra (as shown in Table 2). It should reflect the sum of the first row and should be close to the amount of the bleach, sum of the last row, which is the case here. P-I_1^K converts into P-I_2^{KL}, P-I_3^M, and P-I_4^{fSRI} simultaneously. The amount of P-I_2^{KL} can be obtained from the balance of the first column. The first intermediate is not present in any other b-spectra. The second element of column two, the amplitude of P-I_2^{KL}, is the sum of $fSRI_{620}^K$ and $fSRI_{540}^L$ in the second b-spectrum and should be equal to the amount formed in the first transition. The two numbers are reasonably close, which balances the second row. The rest of the matrix is the same as given by the b-spectra composition. The kinetic matrix calculated from the new V matrix contains only positive rate constants, and its columns are reasonably balanced (Table 5). The matrix describes the kinetics of the transitions shown in Scheme 1:

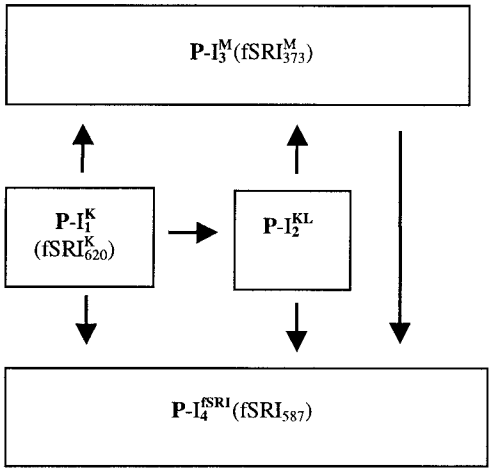

Scheme 1

For the four-exponential fit, the matrix of scaled eigenvectors for the conformational intermediates are shown in Table 6. Here, intermediates P-I_4^M and P-I_5^{fSRI} did not change;

TABLE 4 Eigenvector matrix for the conformational intermediates: three-exponential fit

	b_1	b_2	b_3	b_4
P-I_1^K	102	0	0	0
P-I_2^{KL}	−38	37	0	0
P-I_3^M	−7.6	−15	21	0
P-I_4^{fSRI}	−56	−21	−23	100

TABLE 5 Microscopic rate constants (s^{-1}) of the calculated kinetic matrix for the conformational intermediates: three-exponential fit

	P-I_1^K	P-I_2^{KL}	P-I_3^M	P-I_4^{fSRI}
P-I_1^K	$-2.3\ 10^5$	0	0	0
P-I_2^{KL}	$8.4\ 10^4$	$-5.9\ 10^1$	0	0
P-I_3^M	$1.7\ 10^4$	$2.4\ 10^1$	−1.9	0
P-I_4^{fSRI}	$1.3\ 10^5$	$3.4\ 10^1$	2.1	0

their amounts are the same as already indicated in the composition of the b-spectra. The amounts of the first, second, and third intermediates needed to be recalculated as a result of the new multicolored states. The first element of column 1, the amplitude of P-I_1^K, was calculated in the same way as for the three-exponential fit. P-I_1^K converts into P-I_2^{KL}, P-I_4^M, and P-I_5^{fSRI} simultaneously. Because the first and second decay constants are separated only by a factor of 4, P-I_3^{KL} appears in the b_1-spectrum with a positive amplitude, even though it is not part of the transition (Szundi et al., 1997). Its amount is adjusted to remove any artificial branching from P-I_1^K to P-I_3^{KL}. The amount of P-I_2^{KL} balances the first column. The first intermediate is not present in any other b-spectra. The second element of column two, the amplitude of P-I_2^{KL}, is equal to the amount formed in the first transition, and thus it balances the second row. The amount of P-I_3^{KL} balances the second column. In the third column, there are no P-I_1^K and P-I_2^{KL} present, the amounts of $fSRI_{620}^K$ and $fSRI_{540}^L$ are combined in P-I_3^L. The rest of the matrix is the same as given by the b-spectra composition. The kinetic matrix calculated from the new V matrix contains only positive rate constants, and its columns are reasonably balanced (Table 7). The matrix describes Scheme 2, which is similar to Scheme 1 and shows the splitting of the fast transition into two steps

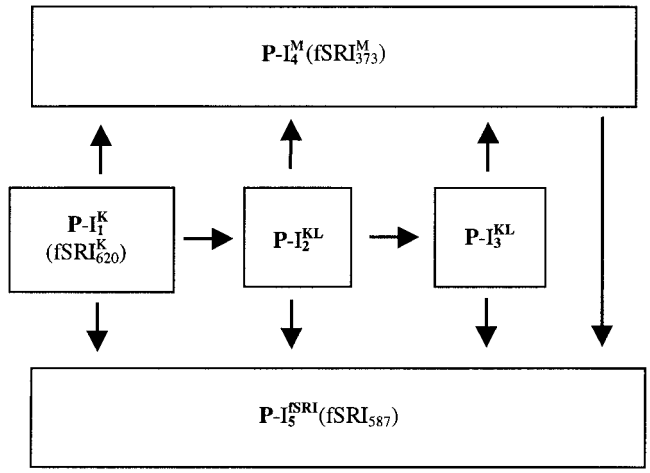

Scheme 2

TABLE 6 Eigenvector matrix for the conformational intermediates: four-exponential fit

	b_1	b_2	b_3	b_4	b_5
P-I_1^K	104	0	0	0	0
P-I_2^{KL}	−75	75	0	0	0
P-I_3^{KL}	12	−50	39	0	0
P-I_4^M	−5.0	−1.0	−17	23	0
P-I_5^{fSRI}	−34	−23	−22	−23	104

The last steps in Scheme 2 can be rearranged to yield Scheme 3:

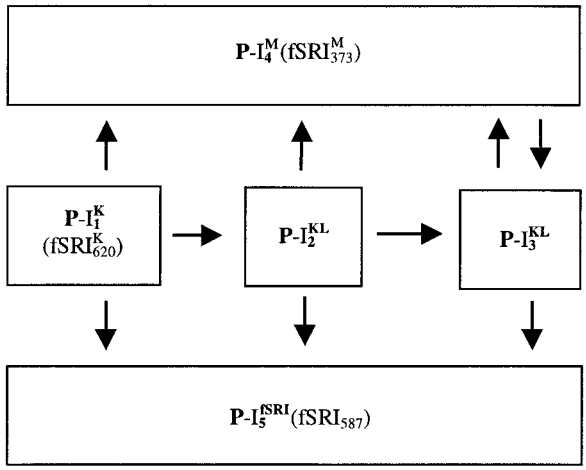

Scheme 3

With the assumption that the equilibrium is shifted to P-I_4^M, Scheme 3 becomes equivalent to Scheme 2 because the third and fourth decay constants in the four-exponential fit are well separated. The back reaction from P-I_4^M to P-I_3^{KL} would be the slow step associated with the fourth exponential decay constant; the other rates are faster. It is easy to realize that with this modification of the scheme, we essentially replaced a single-step transition from P-I_4^M to P-I_5^{fSRI} with a two-step process from P-I_4^M to P-I_3^{KL} to P-I_5^{fSRI}, where the second step is much faster than the first one. Scheme 3 can also be produced by the calculation method used here by introducing a minor P-I_3^{KL} component, at ~1.2 mOD, in the last b-spectrum. The uncertainties in the decomposition do not allow a component of this amplitude to be resolved if the spectra of the components overlap.

TABLE 7 Microscopic rate constants (s^{-1}) of the calculated kinetic matrix for the conformational intermediates: four-exponential fit

	P-I_1^K	P-I_2^{KL}	P-I_3^{KL}	P-I_4^M	P-I_5^{fSRI}
P-I_1^K	$-4.5\ 10^5$	0	0	0	0
P-I_2^{KL}	$2.5\ 10^5$	$-1.1\ 10^5$	0	0	0
P-I_3^{KL}	0	$7.1\ 10^4$	$-6.4\ 10^1$	0	0
P-I_4^M	$2.3\ 10^4$	$1.4\ 10^3$	$2.7\ 10^1$	−1.9	0
P-I_5^{fSRI}	$1.8\ 10^5$	$3.3\ 10^4$	$3.7\ 10^1$	1.9	0

The time-dependent concentrations of the intermediates of Scheme 2 (four-exponential fit) were calculated using the microscopic rate constants in the corresponding kinetic matrix (Table 7). The concentration profiles are shown in Fig. 5 by solid lines. In the first transition from P-I_1^K to P-I_2^{KL}, 40% of the ground form (P-I_5^{fSRI}) recovers. The rest of the ground form recovers in the additional three steps in roughly equal, 20% increments. It is only ~20% of the photoexcited chromophore that finally deprotonates on a millisecond time scale. A similar phenomenon was observed in the photochemistry of SRI below room temperatures (Hazemoto et al., 1983). The K and L color forms are present in more than one of the conformational intermediates. Based on their composition (see below), the second and third conformational intermediates, and the corresponding concentration curves, can be split into these color components. The time-dependent concentrations of the individual K and L color forms, collected from all conformational intermediates, are shown in the figure by dotted lines. The microsecond region clearly shows that the rates of decay and formation of the single-color forms are not single exponentials. The experimental points taken at the red end of the $fSRI_{620}^K$ spectrum, where the contribution of the other color forms is negligible, agree with the slower speed (data not shown). The early M-formation steps originate from the minute and least certain values of $fSRI_{373}^M$ contained in the first two b-spectra. These steps are the least certain, although at least one M-formation step is supported by the balance requirements of the b-spectra decomposition.

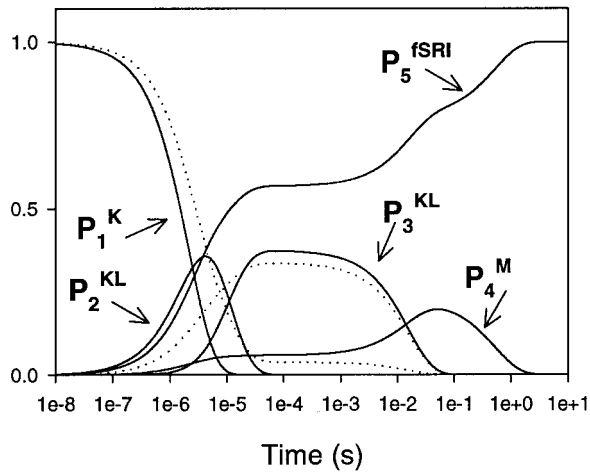

FIGURE 5 Time evolution of the conformational intermediates (——) and the single-colored $fSRI_{620}$ and $fSRI_{540}^L$ forms (· · ·). The concentrations of the intermediates were calculated from the kinetic matrix based on the apparent rates and b-spectra composition of the four-exponential fit, which corresponds to scheme 2. The concentration profiles clearly show the recovery of the ground form (P-I_5^{fSRI}) from the intermediates and the co-existence of the $fSRI_{620}^K$ and $fSRI_{540}^L$ color forms in a broad time window.

Calculation of intermediate spectra

Intermediate spectra containing the bleached spectrum were calculated from the b-spectra and the kinetic matrix. Addition of the ground form spectrum with the appropriate amplitude yielded the absolute spectra of the four conformational intermediates. They were normalized to the ground form spectrum and are shown in Fig. 6. The contributions of $fSRI^{K}_{620}$ and $fSRI^{L}_{540}$ single-colored forms to the spectra of conformational intermediates were determined from spectral decomposition and were found to be 0.66 and 0.34 for $P\text{-}I^{KL}_{2}$ and 0.12 and 0.88 for $P\text{-}I^{KL}_{3}$, respectively. The normalized spectra of the $fSRI^{K}_{620}$, $fSRI^{L}_{540}$ single-colored intermediates derived from the spectra of the conformational intermediate states agree well with the model spectra used in the decomposition of b-spectra, which speaks for the consistency of the analysis.

SUMMARY

The analysis of the photoreaction cycle of transducer-free sensory rhodopsin at low pH revealed a number of interesting features that are not common to the rhodopsin protein family, and gave a detailed kinetic picture of the processes. Shortcuts from intermediates to the ground form are seen rarely at physiological temperatures. SRI in membranes treated with Tween-20 (Ohtani et al., 1988) and SRI below room temperature (Hazemoto et al., 1983) were reported to branch back to the ground form from intermediate states. Also, the formation of the unprotonated Schiff's base in fSRI is suppressed at low pH, and as already reported (Jung et al., 1999), it takes place on a much longer time scale than that of bR or SRI in its natural environment. These phenomena are related to the protonation state of Asp-76 in SRI, which we will present in a future manuscript where we will report the photocycle of this protein at high pH and that of its D76N mutant.

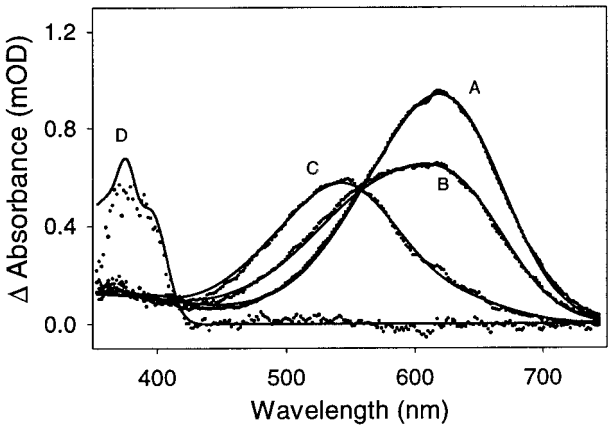

FIGURE 6 Normalized spectra of the conformational intermediates. The experimental spectra (· · ·) were obtained from the b-spectra of the four-exponential fit and the kinetic matrix of scheme 2. The model spectra (——) are constructed from the spectra of the single-colored intermediates. (*Curve A*) Experimental spectrum of $P\text{-}I^{K}_{1}$ and $fSRI^{K}_{620}$ model spectrum. (*Curve B*) Experimental spectrum of $P\text{-}I^{KL}_{2}$ and the sum of 0.66 $fSRI^{K}_{620}$ and 0.34 $fSRI^{L}_{540}$ model spectrum. (*Curve C*) Experimental spectrum of $P\text{-}I^{KL}_{3}$ and the sum of 0.12 $fSRI^{K}_{620}$ and 0.88 $fSRI^{L}_{540}$ model spectrum. (*Curve D*) Experimental spectrum of $P\text{-}I^{M}_{4}$ and $fSRI^{M}_{373}$ model spectrum.

Perhaps the most important result of this paper is the introduction of multicolor conformational states into the fSRI photocycle. Our algebraic method of kinetic analysis proved especially useful to recognize the problems associated with the use of the single-color intermediates and also to derive the corresponding kinetic schemes. The introduction of the multicolor kinetic state is based on the continuous presence of the first intermediate color, which was seen as a small contribution to the spectra at late times. The same types of spectral properties were more pronounced in the D76N fSRI mutant (manuscript in preparation) providing strong support for the interpretation of the b-spectra in this work. It is important to emphasize that the multicolor kinetic states were introduced because the single-color forms that constitute the b-spectra did not produce a physically meaningful kinetic scheme. Multicolor intermediate spectra have been around for a long time because they are easier to produce in a kinetic analysis than to separate them into individual kinetic states with single colors. It is generally accepted that the presence of multiple absorption peaks in intermediate spectra indicates the improper use of oversimplified schemes, and the spectral forms should be, and in many cases are, separable into single peaks by introducing more complexity into the model. Most often this is accomplished by including reversible steps and branches. The kinetic data on bR and bovine rhodopsin typically follow this rule, and a kinetic scheme that produces single-colored intermediates with acceptable standard spectral shapes can be found. When preference is given to the unidirectional sequential model, some of the intermediates in the bR photocycle appear multicolored. With the sequential model, the bR photocycle was recently reinterpreted in terms of multicolor states (Chizhov et al., 1996). As expected, these states appear to be combinations of the consecutive single-color intermediates, which were previously derived by using reversible reaction steps. In our case we cannot introduce reversible steps and branches to separate the colors without sacrificing the shapes of the intermediate spectra. For single-color intermediates having acceptable spectral shapes no kinetic scheme with meaningful microscopic rate constants can be found.

Because any kinetic data set can be explained by implementing enough complexity into the scheme, our conformational model could also be broken down into many steps involving isospectral ground state forms and isospectral intermediates of single color by invoking parallel pathways and very fast equilibrium processes. Multiple ground forms were reported in purified and liposome-reconstituted His-tagged fSRI (Krebs et al., 1995) expressed in halobacteria

and purified fSRI in detergent expressed in *Escherichia coli* (Schmies et al., 2000). Both contain a 400-nm absorbing species that is in a pH-dependent equilibrium mixture with the ground form $fSRI_{587}$. This 400-nm species is presumably the deprotonated all-*trans* Schiff's base. Photochemical behavior of such a heterogeneous system is expected to be complex. In our system, however, there is no evidence for multiple protein forms being present before illumination to justify parallel reaction paths with very similar intermediates evolving on different time scales, as the same protein at high pH apparently shows normal kinetics. We do not favor these complicated schemes, and present here the simpler concept of multicolor states as a physically more justified alternative.

This work was supported in part by National Institutes of Health grant R01-GM43561.

REFERENCES

Ariki, M., Y. Shichida, and T. Yoshizawa. 1987. Low temperature spectrophotometry on the photoreaction cycle of sensory rhodopsin. *FEBS Lett.* 225:255–258.

Blanck, A., D. Oesterhelt, E. Ferrando, E. S. Schegk, and F. Lottspeich. 1989. Primary structure of sensory rhodopsin I, a prokaryotic photoreceptor. *Embo J.* 8:3963–3971.

Bogomolni, R. A., and J. L. Spudich. 1982. Identification of a third rhodopsin-like pigment in phototactic *Halobacterium halobium. Proc. Natl. Acad. Sci. U.S.A.* 79:6250–6254.

Bogomolni, R. A., and J. L. Spudich. 1987. The photochemical reactions of bacterial sensory rhodopsin-I: flash photolysis study in the one microsecond to eight second time window. *Biophys. J.* 52:1071–1075.

Bogomolni, R. A., W. Stoeckenius, I. Szundi, E. Perozo, K. D. Olson, and J. L. Spudich. 1994. Removal of transducer HtrI allows electrogenic proton translocation by sensory rhodopsin I. *Proc. Natl. Acad. Sci. U.S.A.* 91:10188–10192.

Bousché, O., E. N. Spudich, J. L. Spudich, and K. J. Rothschild. 1991. Conformational changes in sensory rhodopsin I: similarities and differences with bacteriorhodopsin, halorhodopsin, and rhodopsin. *Biochemistry.* 30:5395–400.

Chizhov, I., D. S. Chernavskii, M. Engelhard, K. H. Mueller, B. V. Zubov, and B. Hess. 1996. Spectrally silent transitions in the bacteriorhodopsin photocycle. *Biophys. J.* 71:2329–2345.

Fodor, S. P., R. Gebhard, J. Lugtenburg, R. A. Bogomolni, and R. A. Mathies. 1989. Structure of the retinal chromophore in sensory rhodopsin I from resonance Raman spectroscopy. *J. Biol. Chem.* 264: 18280–18283.

Hazemoto, N., N. Kamo, Y. Terayama, Y. Kobatake, and M. Tsuda. 1983. Photochemistry of two rhodopsinlike pigments in bacteriorhodopsin-free mutant of Halobacterium halobium. *Biophys. J.* 44:59–64.

Hoff, W. D., K. H. Jung, and J. L. Spudich. 1997. Molecular mechanism of photosignaling by archaeal sensory rhodopsins. *Annu. Rev. Biophys. Biomol. Struct.* 26:223–258.

Hug, S. J., J. W. Lewis, C. M. Einterz, T. E. Thorgeirsson, and D. S. Kliger. 1990. Nanosecond photolysis of rhodopsin: evidence for a new, blue-shifted intermediate. *Biochemistry.* 29:1475–1485.

Jung, K. H., E. N. Spudich, P. Dag, and J. L. Spudich. 1999. Transducer-binding and transducer-mutations modulate photoactive-site-deprotonation in sensory rhodopsin I. *Biochemistry.* 38:13270–13274.

Krebs, M. P., E. N. Spudich, and J. L. Spudich. 1995. Rapid high-yield purification and liposome reconstitution of polyhistidine-tagged sensory rhodopsin I. *Protein Exp. Purif.* 6:780–788.

Lewis, J. W., and D. S. Kliger. 1993. Microliter flow cell for measurement of irreversible optical absorbance transients. *Rev. Sci. Instr.* 64: 2828–2833.

Lozier, R. H., R. A. Bogomolni, and W. Stoeckenius. 1975. Bacteriorhodopsin: a light-driven proton pump in *Halobacterium halobium*. *Biophys. J.* 15:955–962.

Nagle, J. F. 1991. Solving complex photocycle kinetics: theory and direct method. *Biophys. J.* 59:476–487.

Oesterhelt, D., and W. Stoeckenius. 1973. Functions of a new photoreceptor membrane. *Proc. Natl. Acad. Sci. U.S.A.* 70:2853–2857.

Ohtani, H., T. Kobayashi, and M. Tsuda. 1988. Branching photocycle of sensory rhodopsin in *Halobacterium halobium*. *Biophys. J.,* 53: 493–496.

Olson, K. D., and J. L. Spudich. 1993. Removal of the transducer protein from sensory rhodopsin I exposes sites of proton release and uptake during the receptor photocycle. *Biophys. J.* 65:2578–2585.

Rath, P., K. D. Olson, J. L. Spudich, and K. J. Rothschild. 1994. The Schiff base counterion of bacteriorhodopsin is protonated in sensory rhodopsin I: spectroscopic and functional characterization of the mutated proteins D76N and D76A. *Biochemistry.* 33:5600–5606.

Schmies, G., I. Chizhov, and M. Engelhard. 2000. Functional expression of His-tagged sensory rhodopsin I in *Escherichia coli*. *FEBS Lett.* 466: 67–69.

Schobert, B., and J. K. Lanyi. 1982. Halorhodopsin is a light-driven chloride pump. *J. Biol. Chem.* 257:10306–10313.

Spudich, J. L. 1993. Color sensing in the archaea: a eukaryotic-like receptor coupled to a prokaryotic transducer. *J. Bacteriol.* 175: 7755–7761.

Spudich, E. N., and J. L. Spudich. 1982. Control of transmembrane ion fluxes to select halorhodopsin-deficient and other energy-transduction mutants of *Halobacterium halobium*. *Proc. Natl. Acad. Sci. U.S.A.* 79:4308–4312.

Spudich, E. N., and J. L. Spudich. 1993. The photochemical reactions of sensory rhodopsin I are altered by its transducer. *J. Biol. Chem.* 268: 16095–16097.

Szundi, I., J. W. Lewis, and D. S. Kliger. 1997. Deriving reaction mechanisms from kinetic spectroscopy: application to late rhodopsin intermediates. *Biophys. J.* 73:688–702.

Thorgeirsson, T. E., J. W. Lewis, S. E. Wallace-Williams, and D. S. Kliger. 1992. Photolysis of rhodopsin results in deprotonation of its retinal Schiff's base prior to formation of metarhodopsin II. *Photochem. Photobiol.* 56:1135–1144.

Thorgeirsson, T. E., J. W. Lewis, S. E. Wallace-Williams, and D. S. Kliger. 1993. Effects of temperature on rhodopsin photointermediates from lumirhodopsin to metarhodopsin II. *Biochemistry.* 32:13861–13872.

Yao, V. J., and J. L. Spudich. 1992. Primary structure of an archaebacterial transducer, a methyl-accepting protein associated with sensory rhodopsin I. *Proc. Natl. Acad. Sci. U.S.A.* 89:11915–11919.